Fractionalization in Fractional Correlated Insulating States at $n \pm 1/3$ Filled Twisted Bilayer Graphene

Dan Mao[ORCID],[1] Kevin Zhang,[1] and Eun-Ah Kim[ORCID][1,2,3,4]

[1]*Laboratory of Atomic and Solid State Physics, Cornell University,*
142 Sciences Drive, Ithaca, New York 14853-2501, USA
[2]*Radcliffe Institute for Advanced Study at Harvard, Harvard University,*
10 Garden Street, Cambridge, Massachusetts 02138, USA
[3]*Department of Physics, Harvard University, 17 Oxford Street, Cambridge, Massachusetts 02138, USA*
[4]*Department of Physics, Ewha Womans University, Seoul 03760, Republic of Korea*

Fractionalization without time-reversal symmetry breaking is a long-sought-after goal in the study of correlated phenomena. The earlier proposal of correlated insulating states at $n \pm 1/3$ filling in twisted bilayer graphene and recent experimental observations of insulating states at those fillings strongly suggest that moiré graphene systems provide a new platform to realize time-reversal symmetric fractionalized states. However, the nature of fractional excitations and the effect of quantum fluctuation on the fractional correlated insulating states are unknown. We show that excitations of the fractional correlated insulator phases in the strong coupling limit carry fractional charges and exhibit fractonic restricted mobility. Upon introduction of quantum fluctuations, the resonance of "lemniscate" structured operators drives the system into quantum lemniscate liquid (QLL) or quantum lemniscate solid (QLS). We find an emergent $U(1) \times U(1)$ 1-form symmetry unifies distinct motions of the fractionally charged excitations in the strong coupling limit and in the QLL phase, while providing a new mechanism for fractional excitations in two dimensions. We predict emergent Luttinger liquid behavior upon dilute doping in the strong coupling limit due to restricted mobility and discuss implications at a general $n \pm 1/3$ filling.

Fractionalization, where the quantum number of low-energy excitations is a fraction of the physical constituents (such as electrons), epitomizes strong correlation effects. With reduced phase space amplifying the correlation effects, fractionalization does not require a magnetic field in 1D systems [1–5]. However, in higher dimensions, fractionalization has only been confirmed with breaking of time-reversal symmetry either under fractional quantum Hall settings [6,7] or spontaneous time-reversal symmetry breaking in fractional Chern insulators [8,9]. Theoretical proposals for fractionalization without time-reversal symmetry breaking have invoked the effects of geometric frustration with local constraints, giving rise to emergent gauge theories in spin models and quantum dimer models [10–19]. More recently, the notion of constraints has been taken to new directions with the advent of fracton models characterized by excitations with restricted mobility [20–26]. While exactly solvable models offer theoretical insight [11,20–23], finding a physical realization has been challenging.

The recent observation of time-reversal invariant incompressible states (i.e., zero Chern number) at fractional filling in twisted bilayer graphene [9] presents a new platform for a strongly correlated state at fractional filling. While the nature of the observed states is still largely unknown, two of us predicted that "fidget-spinner"-shaped Wannier orbitals of twisted bilayer graphene can lead to a correlated insulating phase at fractional filling due to the geometric constraints imposed by the shape of the orbitals [27]. While the extensive ground state degeneracy observed in the strong coupling limit [27] implies novel geometrical frustration effects in widely available physical platforms, little is known about the nature of excitations and effects of quantum fluctuations. In this Letter, we evince the fractionalization of doped holes and fractonic nature of the fractionally charged excitations in the strong coupling limit. Furthermore, we derive a resonance in the lemniscate configuration of Wannier orbitals as the leading quantum fluctuation effect that can result in a quantum lemniscate liquid (QLL) or solid (QLS) phase. We find an emergent $U(1) \times U(1)$ 1-form symmetry at low energy and relate the fractonlike behavior of the excitations to the nontrivial string operator under the 1-form symmetry. Finally, we generalize our formalism to other third fillings and twisted trilayer graphene and discuss experimental prospects of detecting the proposed fractionalization.

The model.—The topological obstruction forbids symmetric lattice description of the flat bands of magic angle twisted bilayer graphene [28–35]. However, the common alignment of twisted bilayer graphene with hexagonal
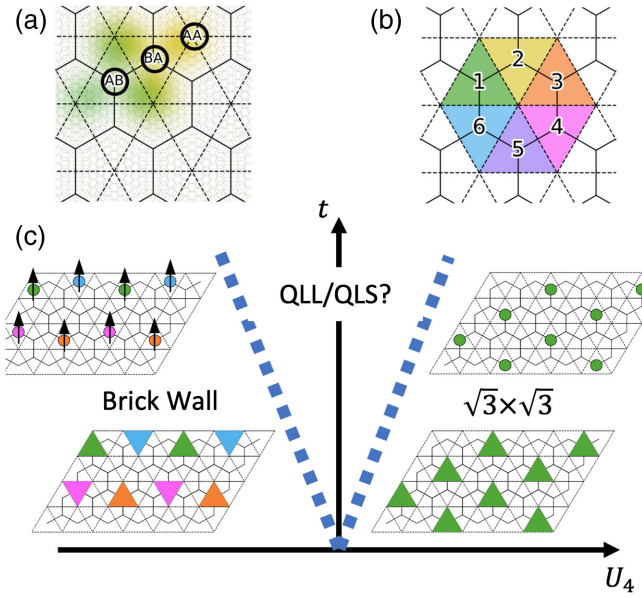
FIG. 1. Wannier states and schematic phase diagram. (a) Wannier states and a typical moiré pattern. The yellow and green blobs schematically represent the shape of Wannier orbitals on the BA and AB sublattices, respectively. (b) Schematic representation of the six-phase registry of AB-BA sites. The vertices of the triangle correspond to the three charge lobes. (c) Proposed phase diagram for the model in Eq. (3). Black arrows in the brick wall phase represent SU(4) spin-valley ferromagnetism.

boron nitride explicitly breaks the C_2 rotational symmetry and justifies construction of Wannier orbitals. Nevertheless, the resulting maximally localized Wannier orbitals are extended beyond their AB-BA site centers [29,36] to the three nearest AA sites, with most of the weight equally divided among the three AA sites, forming a fidget-spinner shape [see Fig. 1(a)]. Consequently, the dominant interaction term is an on-site repulsive interaction projected to the Wannier orbitals taking a "cluster-charging" form [29,37],

$$H_U = \frac{U}{2}\sum_r \left(\sum_{i\in\bigcirc_r} n_i\right)^2, \qquad (1)$$

where $\bigcirc_r$ labels the rth hexagonal plaquette and n_i is summed over spin and valley degrees of freedom.

We note that the convention in the experimental literature is to view the moiré lattice as a triangular lattice with one lattice site per unit cell. On the other hand, the Wannier centers form a honeycomb lattice with two sites per unit cell. Hence, the conventional filling of 1/3 electrons or holes for each spin and valley per triangular lattice is equivalent to the filling fraction of 1/6 per hexagonal lattice per spin and valley [see Fig. 1(a)]. Hereafter, we refer to such filling as 1/3 per moiré unit cell. At such 1/3 total filling for spin and valley degrees of freedom (d.o.f.), the energy can be minimized by having the charge carriers

occupying only one of the six possible registries [see Fig. 1(b)]. Having 1/3 charges per moiré unit cell corresponds to $\sum_{i\in\bigcirc_r} n_i = 1$ per honeycomb plaquette. As pointed out in Ref. [27], the strong coupling limit (i.e., classical) ground state of Eq. (1) is extensively degenerate.

Two types of perturbations can lift the extensive ground state degeneracy associated with the cluster-charging interaction of Eq. (1): further range interactions and quantum fluctuations. For twisted bilayer graphene (TBG) systems, the Coulomb interaction projected to low-energy Wannier orbitals gives rise to various terms [29,38,39]. We focus on the fourth nearest neighbor interactions and consider the density-density interactions and Hund's coupling to obtain [40]

$$H_4 = (V_4 - V_4^{\mathrm{approx}})\sum_{\langle ij\rangle_4} n_i n_j - \frac{J_4}{4}\sum_{\langle ij\rangle_4}(S_i^\mu S_j^\mu + n_i n_j), \qquad (2)$$

where $n_i = c_{i\alpha}^\dagger c_{i\alpha}$ is the density operator summing over the spin and valley d.o.f. and $S^\mu = c_{i,\alpha}^\dagger T_{\alpha\beta}^\mu c_{j,\beta}$ is the SU(4) spin operator; α, β denote the combined spin-valley d.o.f. with the SU(4) generators $T^\mu \in \{\sigma^\nu, \tau^{\nu'}, \sigma^\nu \otimes \tau^{\nu'}\}$. Following the notation of Ref. [30], V_4 (V_4^{approx}) is the direct Coulomb interaction between fourth nearest neighbor ("point-charge-approximated") Wannier orbitals. The point-charge approximation [30] views the fidget-spinner-shaped Wannier orbitals as being composed of three point charges at AA sites. Focusing on Eq. (2) is justified by the fact that the difference between the direct Coulomb interaction and the point-charge approximation is short ranged, while all tiling patterns in the ground state manifold of Eq. (1) have the same electrostatic potential under the point-charge approximation. Finally, $J_4 > 0$ is the SU(4) ferromagnetic exchange interaction [38]. Upon introducing quantum fluctuations via hopping term $H_K = \sum_{\langle ij\rangle,\alpha,\tau} t_{ij,\tau}(c_{i,\alpha,\tau}^\dagger c_{j,\alpha,\tau} + \mathrm{H.c.})$, the full Hamiltonian becomes

$$H = H_U + H_4 + H_K. \qquad (3)$$

The ground states in the strong coupling limit ($t = 0$) were established in Ref. [27]. With finite hopping t, quantum order by disorder [50] would select a different quantum ground state, resulting in a qualitative phase diagram we sketch in Fig. 1(c).

Strong coupling limit and fractional excitations.—In the strong coupling limit, the characteristic energy scale is

$$U_4 = V_4 - V_4^{\mathrm{approx}} - \frac{J_4}{2}. \qquad (4)$$

For $U_4 < 0$, the system will order into a low-symmetry state dubbed the "brick wall" [27] [Fig. 1(c)]. The brick wall tiling makes the maximal use of Hund's coupling to minimize H_4 and will thus be an SU(4) spin-valley

ferromagnet. The anisotropic shape of the mesoscale unit results in low symmetry. Translation, mirror, and C_3 rotation symmetries of the honeycomb lattice are all broken in the brick wall phase. From the point of view of the Wannier orbital centers [circles in Fig. 1(c)], the brick wall state is closely related to the stripe ordered phase proposed in Ref. [38] at filling $n = -3$ of TBG since the brick wall occupies every third site along a stripe. Hence, the brick wall may be favored at 1/3 filling away from $n = -3$. On the other hand, for $U_4 > 0$, the favored state would be the $\sqrt{3} \times \sqrt{3}$ ordered state, with uniform AB-BA registry. In this case, from Eq. (2), configurations with different spin-valley orientations are degenerate within the model. While the two states break translational symmetry in terms of the orbital centers [see filled circles in Fig. 1(c)], we anticipate the observable effects of the translational symmetry breaking to be weak due to the spread of the Wannier orbitals. This contrasts the proposed $\sqrt{3} \times \sqrt{3}$ state against the unit-cell tripled charge density wave states proposed in momentum space based numerical approaches [51,52].

A natural consequence of the incompressible tiling in the strong coupling limit at $\pm 1/3$ filling is the possibility of fractionally charged holes. Intuitively, this can be anticipated by noting that 1/3 of the electron charge is concentrated at the vertices of the dual triangular lattice for any of the incompressible states [30]. The configuration that binds a 1/3 charge and the energy cost of such an excitation depends on the classical ground state. However, as we show below, their movements are restricted much like fractons and lineons [23,25,26].

The $\sqrt{3} \times \sqrt{3}$ phase has two types of charge 1/3 fractional excitations with restricted mobility: vortices [Fig. 2(a)] and solitons [Fig. 2(b)]. As it was previously noted [53], a vortex of phase registry in a charge ordered state usually carries fractional charge. An unusual property of our vortices is their restricted mobility: the cluster charging energy U makes the vortices practically immobile, similar to fractons [23,24]. However, due to the extensive energy cost proportional to U_4 associated with the domain walls, the observation of these vortices would require finite temperature. We define a soliton of the $\sqrt{3} \times \sqrt{3}$ phase to be the 1/3 charged excitation bound to the end of a line of flipped trimers. In the limit of vanishingly small U_4, a single hole can fractionalize into three solitons that can only move along one dimension associated with the flip line. The soliton dynamics are as if a domain wall state of the Su-Schrieffer-Heeger model [1] were embedded in a two-dimensional space. Hence, the soliton behaves like a lineon [23,24]. However, the solitons in the $\sqrt{3} \times \sqrt{3}$ state are confined. The balance between the flip-line energy cost ($2U_4$ per flip) and the Coulomb interaction between the 1/3 charges determines the size of the bound state. From the estimation of U_4 in Ref. [54], we have $L \sim 1.13 a_M$ (see Supplemental Material, Sec. B for detailed discussion [40]).
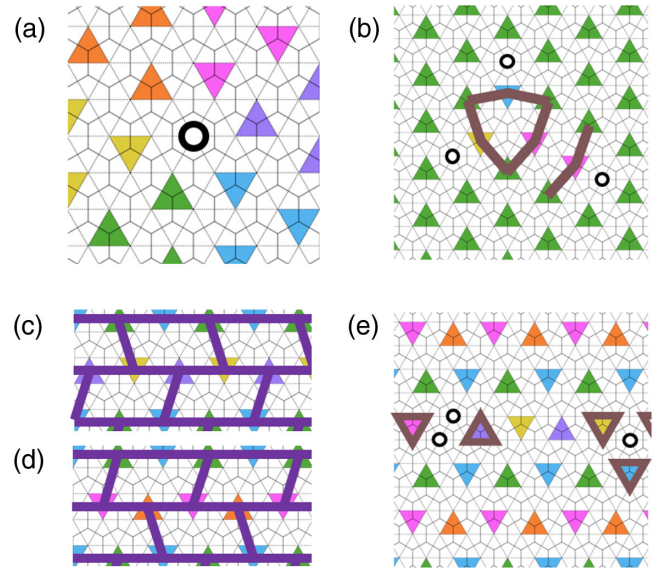

FIG. 2. Fractionally charged excitations. (a) A single 1/3 charged vacancy (open circle), surrounded by all six registry domains. (b) Three solitons with 1/3 charge and flip-line tails. The brown lines indicate the energy cost U_4 associated with the domain walls. (c),(d) Two degenerate brick wall states. (e) Solitons in the brick wall phase can move along a 1D line with constant energy cost associated with brown triangles.

Solitons in the brick wall phase are more intriguing because they are deconfined. First we note that, as shown in Figs. 2(c) and 2(d), the brick wall phase has subextensive ground state degeneracy since each line of "bricks" can choose between two degenerate choices of alternating registries that give different slants to the brick tiling pattern. Hence, the ground state degeneracy is 3×2^L where L is the linear dimension, and the configurational entropy is $L \log 2$ [55]. A defect associated with a domain boundary within a row can also be viewed as a soliton carrying 1/3 charge [Fig. 2(e)] or 2/3 charge (see Supplemental Material, Sec. B). Similar to the $\sqrt{3} \times \sqrt{3}$ phase, the solitons in the brick wall phase also have restricted mobility and can only move along the one dimension of the brick wall rows, which are 2D analogs to the lineon excitations in the 3D X-cube model [23,24]. Furthermore, the solitons in the brick wall phase are deconfined excitations since they cost a finite energy irrespective of the separation between the solitons [see Fig. 2(e) and a more detailed illustration in Supplemental Material, Sec. B].

The restricted mobility of the solitons seems to happen by chance at first glance. However, as we will show later, these properties are robust against small quantum fluctuations and are closely related to emergent symmetries at low energy.

Quantum fluctuations.—We now turn to the vertical axis of the phase diagram [Fig. 1(c)] and explore the effects of quantum fluctuations in the limit of $U_4 \ll t$. We ask how the hopping t in H_K would lift the extensive degeneracy of
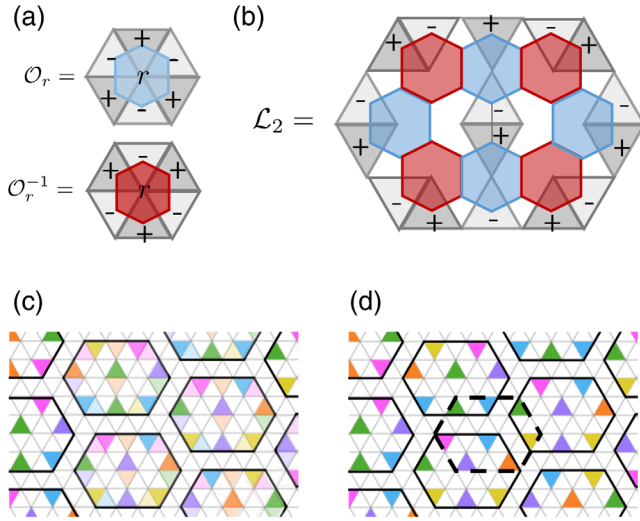
FIG. 3. Operators in effective Hamiltonian (5) and QLS. (a) The lowest order term consists of a plaquette operator $\mathcal{O}_r$. The annihilation (creation) operator acts on the sites marked by $-(+)$ symbols. (b) The lowest order nonvanishing operator L_2 spans ten plaquettes. (c) The plaquettelike candidate state for the QLS, where the resonance happens between the darker shaded triangles and lighter shaded ones. (d) The columnarlike state. The dotted hexagon denotes an extra flippable pattern when the surrounding three states are all aligned.

the H_U ground state manifold through quantum "order from disorder" [50]. To start answering this question, we look for an operator that can locally connect two different states in the classical ground state manifold. Such operator should commute with H_U, i.e., keep the cluster charge fixed. Moreover, the operator should act nontrivially in the ground state manifold of H_U at filling $n = \pm 1/3$, without annihilating the states in the manifold. Since the ground state manifold of H_U at filling $n = \pm 1/3$ consists of states with exactly one site of the hexagonal cluster occupied, connecting such states requires coordinated multisite hopping. We now show that the smallest such operator consists of an eight-site hopping arranged in a lemniscate, or sideways figure-eight shape [see Fig. 3(b)].

The lemniscate operator $\mathcal{L}_2$ is constructed from the intrahexagon hopping operator $\mathcal{O}_\bigcirc = c_{i_1}^\dagger c_{i_2} c_{i_3}^\dagger c_{i_4} c_{i_5}^\dagger c_{i_6}$, where $i_{1,\ldots,6}$ label the sites belonging to a hexagonal plaquette, organized in a clockwise order [Fig. 3(a)]. Clearly, $[\mathcal{O}_\bigcirc, H_U] = 0$, but $\mathcal{O}_\bigcirc |\psi_0\rangle = 0$ for any $|\psi_0\rangle$ in the ground state manifold of H_U at filling $n = \pm 1/3$, since $\mathcal{O}_\bigcirc$ annihilates three fermions on a hexagon, but the cluster-charging constraint requires exactly one fermion on each hexagon. However, a larger structure involving multiple hexagons built from alternating $\mathcal{O}_\bigcirc$ and $\mathcal{O}_\bigcirc^{-1}$ operators would still commute with H_U and can be made to be compatible with the cluster-charging constraint. The lemniscate operator $\mathcal{L}_2$ illustrated in Fig. 3(b) is the smallest operator (see Supplemental Material, Sec. C [40]) that can semilocally resonate between two different states

in the classical ground state manifold. There are three orientations of lemniscate operators, related by C_3 rotation. For each orientation, the lemniscate operator connects two local tiling configurations, which we designate as the "flippable" manifold of that operator. Therefore, the low-energy effective Hamiltonian can be written as

$$H_{\text{eff}} = -\tilde{t} \sum_{i,\alpha} (\mathcal{L}_{2,i,\alpha} + \mathcal{L}_{2,i,\alpha}^\dagger) + H_4, \qquad (5)$$

where $\tilde{t} \sim t^8/U^7$, $\alpha \in \{1, 2, 3\}$ label the three different orientations, and i labels the position of the operator $\mathcal{L}_2$ [Fig. 3(b)].

The effective Hamiltonian H_{eff} is highly frustrated since different $\mathcal{L}_{2,i,\alpha}$'s do not commute. Nevertheless, analogies to the quantum dimer models [56] offer valuable insights. Specifically, as in quantum dimer models, the quantum fluctuations associated with the lemniscate operators would select a novel quantum liquid state or a solid state as a function of $U_4/\tilde{t}$; we refer to these states as quantum lemniscate liquid or solid [Fig. 1(c)]. The quantum fluctuation through the lemniscate operators will avoid any mobility restriction for doped charges in both phases.

Among possible QLS states are a plaquettelike state that has resonance within supercells [Fig. 3(c)] and a columnar-like state with fixed configurations within supercells that repeats for $U_4 < 0$ [Fig. 3(d)] or alternates for $U_4 > 0$. Both the plaquette- and columnarlike QLS states break C_3 rotational symmetry in addition to the lattice translation symmetry. The supercells act as emergent local degrees of freedom analogous to the emergent orbitals in the so-called cluster Mott insulators on the kagome lattice [57]. However, while such emergent orbitals are pinned to the lattice, our supercells form an emergent superstructure in the QLS. Doping away from $1/3$ filling, holes added to the QLS phases can also fractionalize into $1/3$ charged excitations. However, they are energetically confined as in the $\sqrt{3} \times \sqrt{3}$ phase (see Supplemental Material, Sec. C [40]).

While mapping out the conditions for the QLL ground state of the Hamiltonian (5) would require numerical or quantum simulation of the model, some properties of a QLL state can be anticipated on general grounds. One mechanism that would favor a QLL over a QLS state is through resonances unconstrained to a rigid cell [e.g., the dotted hexagon in Fig. 3(d)]. As we describe using a minimal effective model in the Supplemental Material, Sec. D [40], such resonance will promote a QLL state that breaks the C_3 rotational symmetry. A gapped and translationally invariant QLL state must host deconfined charge $1/3$ anyonic excitations based on Lieb-Schultz-Mattis–type constraints [58]. Such excitations can be viewed as the $1/3$ charged lineons becoming fully mobile due to lemniscate resonances. Alternatively, a QLL analogous to the valence bond liquid state at the so-called Rokhsar-Kivelson

point [11,15] would be an equal weight superposition of all the possible tiling configurations. Such a QLL state will respect C_3 rotation symmetry.

Emergent 1-form symmetry.—We turn to the theoretical implications of the fractonic restricted mobility of our fractionally charged defects. It is believed that fracton phases do not exist in fully gapped systems in two spatial dimensions [21], without symmetry protection. However subsystem symmetry [59–61] or multipolar symmetry [62–64] can result in fractonic excitations with restricted mobility in 2D [65]. Curiously, we find the mobility restriction of fractional charge in our model is tied to a new emergent 1-form symmetry; a new mechanism for fractonic excitations in 2D.

The notion of p-form symmetry, a symmetry operator acting on codimension-$(p + 1)$ submanifold of the space-time, has garnered interest in the community as a framework that unifies the Landau symmetry breaking paradigm with topologically ordered phases [65]. As we prove in the Supplemental Material, Sec. F [40], the cluster charging constraint implies an emergent $U(1) \times U(1)$ 1-form symmetry at low energy (see Supplemental Material [40]). The string operator charged under the symmetry moves the fractionally charged excitation from one end to the other. This 1-form symmetry unifies the distinct descriptions of fractional charge motion as follows. In the brick wall and $\sqrt{3} \times \sqrt{3}$ phases, the string operators are rigid, resulting in restricted mobility of the lineons. Contrastingly, in the QLL phase, the string operator is allowed to fluctuate, resulting in unrestricted motion of the fractional charge.

Experimental implications.—Our rich phase diagram with exotic states in experimentally accessible platform opens the door for detection and control of novel states. The restricted mobility of lineons in the brick wall phase gives rise to emergent Luttinger liquid behavior at small hole doping away from filling of 1/3. The lineon motion can be modeled using three flavors of solitons. In contrast to the well-studied commensurate-incommensurate transition near 1/3 filling in one dimension predicted to exhibit the Luttinger parameter $K = 1/9$ [41], we predict the Luttinger parameter, the emergent lineon Luttinger liquid, to be $K = 1/3$ (see Supplemental Material [40]). The prediction can be verified through Luttinger liquid scaling of conductance and a violation of Wiedemann-Franz law and divergent Lorentz number at low temperature (see Supplemental Material, Sec. E).

More broadly, our formalism can be generalized and applied to other third fillings by accommodating more electrons per honeycomb plaquette (see Supplemental Material, Sec. G). Furthermore, since the geometry of the extended orbital does not require the fine-tuning of the magic angle, we anticipate the fractional incompressible states at $n \pm 1/3$ to be robustly present even at larger twist angles [66].

For fillings larger than 1, some sites will have double occupation, resulting in a competition between spin-singlet, valley-polarized, and spin-triplet, valley-antialigned states. Switching between competing states will manifest through nonmonotonic magnetotransport under an in-plane field.

Finally, mirror-symmetric twisted trilayer graphene at 1/3 filling can host a fractional correlated insulating state presented in this Letter with an additional Dirac cone at charge neutrality (see Supplemental Material [40]). Interestingly, recent experiments on twisted trilayer graphene reported observation of zero Chern number incompressible states [67].

[1] W. P. Su, J. R. Schrieffer, and A. J. Heeger, Phys. Rev. Lett. **42,** 1698 (1979).

[2] K.-V. Pham, M. Gabay, and P. Lederer, Phys. Rev. B **61,** 16397 (2000).

[3] K.-I. Imura, K.-V. Pham, P. Lederer, and F. Piéchon, Phys. Rev. B **66,** 035313 (2002).

[4] D. Orgad, S. A. Kivelson, E. W. Carlson, V. J. Emery, X. J. Zhou, and Z. X. Shen, Phys. Rev. Lett. **86,** 4362 (2001).

[5] H. Steinberg, G. Barak, A. Yacoby, L. N. Pfeiffer, K. W. West, B. I. Halperin, and K. Le Hur, Nat. Phys. **4,** 116 (2008).

[6] R. B. Laughlin, Phys. Rev. Lett. **50,** 1395 (1983).

[7] J. Martin, S. Ilani, B. Verdene, J. Smet, V. Umansky, D. Mahalu, D. Schuh, G. Abstreiter, and A. Yacoby, Science **305,** 980 (2004).

[8] N. Regnault and B. A. Bernevig, Phys. Rev. X **1,** 021014 (2011).

[9] Y. Xie, A. T. Pierce, J. M. Park, D. E. Parker, E. Khalaf, P. Ledwith, Y. Cao, S. H. Lee, S. Chen, P. R. Forrester, K. Watanabe, T. Taniguchi, A. Vishwanath, P. Jarillo-Herrero, and A. Yacoby, Nature (London) **600,** 439 (2021).

[10] P. W. Anderson, Science **235,** 1196 (1987).

[11] D. S. Rokhsar and S. A. Kivelson, Phys. Rev. Lett. **61,** 2376 (1988).

[12] I. Affleck and J. B. Marston, Phys. Rev. B **37,** 3774 (1988).

[13] N. Read and S. Sachdev, Phys. Rev. Lett. **66,** 1773 (1991).

[14] X. G. Wen, Phys. Rev. B **44,** 2664 (1991).

[15] R. Moessner and S. L. Sondhi, Phys. Rev. Lett. **86,** 1881 (2001).

[16] T. Senthil and M. P. A. Fisher, Phys. Rev. B **62,** 7850 (2000).

[17] A. Kitaev, Ann. Phys. (Amsterdam) **303**, 2 (2003).

[18] A. Kitaev, Ann. Phys. (Amsterdam) **321**, 2 (2006).

[19] C. Castelnovo, R. Moessner, and S. L. Sondhi, Nature (London) **451**, 42 (2008).

[20] C. Chamon, Phys. Rev. Lett. **94**, 040402 (2005).

[21] J. Haah, Phys. Rev. A **83**, 042330 (2011).

[22] B. Yoshida, Phys. Rev. B **88**, 125122 (2013).

[23] S. Vijay, J. Haah, and L. Fu, Phys. Rev. B **92**, 235136 (2015).

[24] S. Vijay, J. Haah, and L. Fu, Phys. Rev. B **94**, 235157 (2016).

[25] R. M. Nandkishore and M. Hermele, Annu. Rev. Condens. Matter Phys. **10**, 295 (2019).

[26] M. Pretko, X. Chen, and Y. You, Int. J. Mod. Phys. A **35**, 2030003 (2020).

[27] K. Zhang, Y. Zhang, L. Fu, and E.-A. Kim, Commun. Phys. **5**, 250 (2022).

[28] L. Zou, H. C. Po, A. Vishwanath, and T. Senthil, Phys. Rev. B **98**, 085435 (2018).

[29] H. C. Po, L. Zou, A. Vishwanath, and T. Senthil, Phys. Rev. X **8**, 031089 (2018).

[30] M. Koshino, N. F. Q. Yuan, T. Koretsune, M. Ochi, K. Kuroki, and L. Fu, Phys. Rev. X **8**, 031087 (2018).

[31] J. Kang and O. Vafek, Phys. Rev. X **8**, 031088 (2018).

[32] J. Ahn, S. Park, and B.-J. Yang, Phys. Rev. X **9**, 021013 (2019).

[33] Z. Song, Z. Wang, W. Shi, G. Li, C. Fang, and B. A. Bernevig, Phys. Rev. Lett. **123**, 036401 (2019).

[34] J. Liu, J. Liu, and X. Dai, Phys. Rev. B **99**, 155415 (2019).

[35] Z.-D. Song, B. Lian, N. Regnault, and B. A. Bernevig, Phys. Rev. B **103**, 205412 (2021).

[36] N. F. Q. Yuan and L. Fu, Phys. Rev. B **98**, 045103 (2018).

[37] O. I. Motrunich and T. Senthil, Phys. Rev. Lett. **89**, 277004 (2002).

[38] J. Kang and O. Vafek, Phys. Rev. Lett. **122**, 246401 (2019).

[39] Y.-H. Zhang, D. Mao, and T. Senthil, Phys. Rev. Res. **1**, 033126 (2019).

[40] See Supplemental Material at http://link.aps.org/supplemental/10.1103/PhysRevLett.131.106801 for detailed discussion on fractional excitations and their confinement properties, which includes Refs. [30,38,41–49].

[41] T. Giamarchi, *Quantum Physics in One Dimension* (Clarendon Press, Oxford, 2003), Vol. 121.

[42] P. P. Ewald, Ann. Phys. (Berlin) **369**, 253 (1921).

[43] S. D. Pace and X.-G. Wen, arxiv:2301.05261.

[44] C. L. Kane and M. P. A. Fisher, Phys. Rev. Lett. **68**, 1220 (1992).

[45] C. L. Kane and M. P. A. Fisher, Phys. Rev. B **46**, 15233 (1992).

[46] A. Georges, T. Giamarchi, and N. Sandler, Phys. Rev. B **61**, 16393 (2000).

[47] C. L. Kane and M. P. A. Fisher, Phys. Rev. Lett. **76**, 3192 (1996).

[48] M.-R. Li and E. Orignac, Europhys. Lett. **60**, 432 (2002).

[49] E. Khalaf, A. J. Kruchkov, G. Tarnopolsky, and A. Vishwanath, Phys. Rev. B **100**, 085109 (2019).

[50] C. L. Henley, Phys. Rev. Lett. **62**, 2056 (1989).

[51] P. Wilhelm, T. C. Lang, and A. M. Läuchli, Phys. Rev. B **103**, 125406 (2021).

[52] S. Zhang, X. Lu, and J. Liu, Phys. Rev. Lett. **128**, 247402 (2022).

[53] L. Balents, L. Bartosch, A. Burkov, S. Sachdev, and K. Sengupta, Phys. Rev. B **71**, 144508 (2005).

[54] M. Koshino, N. F. Q. Yuan, T. Koretsune, M. Ochi, K. Kuroki, and L. Fu, Phys. Rev. X **8**, 031087 (2018).

[55] The subextensive degeneracy is not topologically protected and can be split by further range interactions (see [40]).

[56] R. Moessner, S. L. Sondhi, and P. Chandra, Phys. Rev. B **64**, 144416 (2001).

[57] G. Chen and P. A. Lee, Phys. Rev. B **97**, 035124 (2018).

[58] M. Cheng, M. Zaletel, M. Barkeshli, A. Vishwanath, and P. Bonderson, Phys. Rev. X **6**, 041068 (2016).

[59] M. Qi, L. Radzihovsky, and M. Hermele, Ann. Phys. (Amsterdam) **424**, 168360 (2021).

[60] X. Shen, Z. Wu, L. Li, Z. Qin, and H. Yao, Phys. Rev. Res. **4**, L032008 (2022).

[61] B. C. Rayhaun and D. J. Williamson, arXiv:2112.12735.

[62] M. Pretko, Phys. Rev. B **95**, 115139 (2017).

[63] M. Pretko, Phys. Rev. B **96**, 035119 (2017).

[64] M. Pretko and L. Radzihovsky, Phys. Rev. Lett. **120**, 195301 (2018).

[65] J. McGreevy, Annu. Rev. Condens. Matter Phys. **14**, 57 (2023).

[66] H. Tian, E. Codecido, K. Zhang, D. Mao, E.-A. Kim, M. Bockrath, and C. Lau (unpublished).

[67] C. Shen, P. J. Ledwith, K. Watanabe, T. Taniguchi, E. Khalaf, A. Vishwanath, and D. K. Efetov, Nat. Mater. **22**, 316 (2023).